Supplementary Data

Details of Experimental Methods

Flow Cell Fabrication and Assembly

The flow cell was fabricated from polycarbonate blocks (l = 50 mm, w = 50 mm, h = 6 mm). The body of the flow cell was fabricated by milling out a fluid channel (l = 30 mm, w = 2 mm, h = 2 mm) in a polycarbonate block. A channel for mounting the resonator (l = 10 mm, w = 2 mm, d = 1 mm) was established at one end of the main channel, and a perpendicular channel for mounting the waveguide (l = 50 mm, w = 2 mm, d = 1 mm) was also created. A lid was fabricated using a similar polycarbonate block with 6-32 tapped holes aligned to the ends of the main channel, which served as the inlet and outlet ports. Female Luer connectors with 6-32 tapped ends were threaded into the inlet and outlet ports and sealed with hot glue.

Because the waveguides were extremely fragile, they could not be removed from the syringe pump without breaking. Instead, the flow cell was attached to a 3-axis micromanipulator (Newport, Irvine, CA) and moved under the waveguide so that the cross-channel of the flow cell was aligned to the waveguide and the narrowest region of the waveguide was centered in the main fluidic channel. The micromanipulator was used to raise the flow cell until the waveguide rested on the bottom of the waveguide channel. The waveguide was then sealed in place with Kwik-sil silicon elastomer adhesive (World Precision Instruments Inc., Sarasota, FL). After the adhesive was set (approximately 10 minutes) the waveguide was removed from the syringe pump and spliced into the fiber between the laser and the detector. With the laser, detector and data acquisition system running, a silane-coated microsphere was attached to another

3-axis micromanipulator and aligned over the waveguide. The microsphere was slowly lowered into contact with the tapered section of the waveguide. Upon contact with the waveguide, resonances could be observed in the spectrum on the data acquisition VI. The microsphere was aligned so that it was centered in the fluid channel, the stalk of the resonator rested on the bottom of the microsphere channel, and deep resonances were observed on the spectrum. The microsphere was then secured into place using Kwik-sil elastomer adhesive and the nitrous-butane was used to sever the stalk of the resonator without disturbing its alignment with the waveguide. The gain on the DAQ card and detector were then adjusted to optimize the signal to noise ratio.

After the adhesive had set the channels in the flow cell were primed with 50 mM PBS (pH 7.4). Priming the channels ensured that no bubbles would be present in the flow cell when it was sealed. A 1 mm thick PDMS gasket was placed between the lid and the body of the flow cell. The body of the flow cell was placed on an aluminum base with four threaded studs. The gasket was placed on the body and the lid was placed over the gasket. The studs passed through holes in the flow cell body, gasket, and lid. Wing nuts with washers were used to seal the flow cell by applying even compression across the lid. More PBS was added through the inlet port using a hypodermic needle and syringe to displace the air remaining in the flow cell before the tubing was connected.

Data analysis

Binary files saved by the LabView data acquisition software were analyzed offline using a data analysis algorithm implemented in Python. The algorithm reconstructed the spectral location (in nm) of each resonance over time. The resonance with the lowest

FWHM value and a continuous trace over the entire time span was chosen for further analysis. Any drift in the baseline data was corrected by subtracting a linear function from the data. The surface concentration of the adsorbed species σ_s is related to the measured change in resonant wavelength Δλ by:

$$\frac{\Delta\lambda}{\lambda} = \frac{\alpha_{ex}\,\sigma_s}{\varepsilon_0\left(n_s^2 - n_m^2\right)R} \qquad 7$$

λ is the nominal wavelength of the resonance, Δλ is the wavelength shift of the resonance, n_s is the refractive index of the sphere (1.46)[54], n_m is the refractive index of the medium surrounding the sphere (1.3357)[55], ε_o is the permittivity of free space, and *R* is the radius of the spheroid. Spheroid radii were measured from images taken by brightfield microscopy. α_{ex} is the excess polarizability of the protein molecule, which can be calculated from the refractive index increment *dn/dc* according to:

$$\alpha_{ex} = \varepsilon_0 2 n_m \frac{dn}{dc} m \qquad 8$$

The refractive index increment *dn/dc* for proteins such as GO in dilute solutions is ~0.184 cm^3/g[34, 56] and m is the mass of a single molecule of GO. Equations 7 and 8 were combined to obtain

$$\sigma_s = \frac{\Delta\lambda}{\lambda}\frac{\left(n_s^2 - n_m^2\right)R}{2n_m\, dn/dc\, m} \qquad 9$$

This result was used to obtain the surface density (ng/cm^2) of adsorbed protein:

$$\rho_s = \sigma_s m = \frac{\Delta\lambda}{\lambda}\frac{\left(n_s^2 - n_m^2\right)R}{2n_m\, dn/dc} \qquad 10$$

Note that the mass of GO was not required for this calculation, so that uncertainties in the molar mass of GO did not impact the surface density reported by the WGM biosensor.

Modeling Methods

Blocking Function for RSA Model

Since the blocking function for the random sequential adsorption (RSA) of spherical particles was not available in analytic form, a polynomial approximation for the blocking function was used[30]:

$$\Phi(\theta) = \frac{\left(1-\bar{\theta}\right)^3}{1.0 - 0.812\bar{\theta} + 0.2335\bar{\theta}^2 + 0.0845\,\bar{\theta}^3} \qquad 11$$

$\bar{\theta} = \theta/\theta_\infty$ and $\theta_\infty \approx 0.547$.

Two-stage RSA-Type Model with Post-Adsorption Transition

Scaled particle theory has been used to obtain approximations to the blocking functions for the adsorption of spherical particles with a post-adsorption transition[32]. In that reference, the following kinetic equations were defined:

$$\frac{d\rho_\alpha}{dt} = k_a c\Phi_\alpha - k_s\rho_\alpha\Psi_{\alpha\beta} - k_d\rho_\alpha \qquad 12$$

$$\frac{d\rho_\beta}{dt} = k_s\rho_\alpha\Psi_{\alpha\beta} \qquad 13$$

A common notation must be used to compare the various adsorption models quantitatively. The surface number densities ρ_i used in equations 12 and 13 were converted to fractional surface coverage using $\theta_i = \sigma_i\rho_i$, where σ_i is the area covered by one adsorbed particle, to obtain:

$$\frac{d\theta_\alpha}{dt} = k_a c\Phi_\alpha - k_s\theta_\alpha\Psi_{\alpha\beta} - k_d\theta_\alpha \qquad 14$$

$$\frac{d\theta_\beta}{dt} = k_s\Sigma^2\theta_\alpha\Psi_{\alpha\beta} \qquad 15$$

When $k_s = 0$, equations 14 and 15 reduced to equation 2.

The form of the blocking functions depends upon the assumptions of the model. When the particles are spherical, scaled particle theory (SPT) can be used to derive the following blocking functions:

$$\Phi_\alpha = (1-\theta)\exp\left[-\frac{2\left(\bar{\rho}_\alpha + \Sigma\bar{\rho}_\beta\right)}{1-\theta} - \frac{\bar{\rho}_\alpha + \bar{\rho}_\beta + (\Sigma-1)^2\bar{\rho}_\alpha\bar{\rho}_\beta}{(1-\theta)^2}\right] \qquad 16$$

$$\Psi_{\alpha\beta} = \exp\left[-\frac{2(\Sigma-1)\left(\bar{\rho}_\alpha + \Sigma\bar{\rho}_\beta\right)}{1-\theta} - \frac{\left(\Sigma^2-1\right)\left[\bar{\rho}_\alpha + \bar{\rho}_\beta + (\Sigma-1)^2\bar{\rho}_\alpha\bar{\rho}_\beta\right]}{(1-\theta)^2}\right] \qquad 17$$

The following non-dimensional variables were defined: $\bar{\rho}_\alpha = \rho_\alpha\pi R_\alpha^2$, $\bar{\rho}_\beta = \rho_\beta\pi R_\alpha^2$, $\Sigma = R_\beta / R_\alpha$ and $\theta = \bar{\rho}_\alpha + \Sigma^2\rho_\chi$. Since the blocking functions derived from SPT describe spherical particles, they could be directly compared to the RSA blocking function. Supporting Figure 1 shows that the blocking function Φ_α was similar but not identical to the RSA blocking function defined by Equation 11.

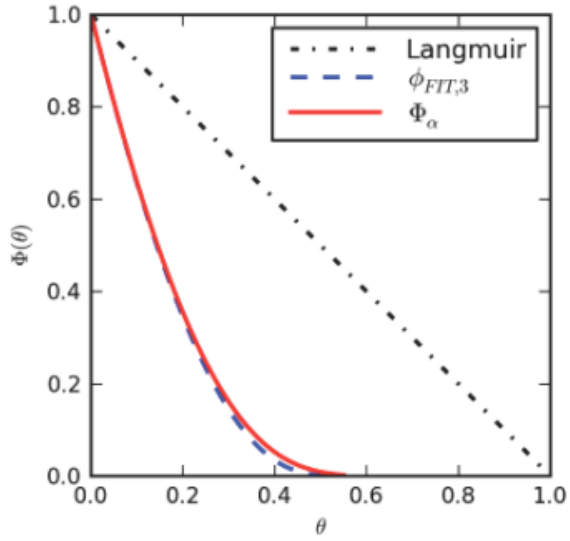

Supporting Figure 1. Comparison of the RSA blocking function, the blocking function Φ_α for the adsorption model with post-adsorption transition derived from scaled particle theory, and the Langmuir blocking function.

Two-stage Langmuir-Type Model with Post-Adsorption Transition

A different model of adsorption with a post-adsorption transition has been proposed[31] and used to fit the adsorption kinetics of the fibronectin fragment $FNIII_{7\text{-}10}$.[33] Written using the same variables as equations 12 and 13, the equations that describe this model are

$$\frac{d\rho_\alpha}{dt} = k_a c A_{av} - k_s \rho_\alpha A_{av} - k_d \rho_\alpha \qquad 18$$

$$\frac{d\rho_\beta}{dt} = k_s \rho_\alpha A_{av} \qquad 19$$

where ρ_i is the surface density (*ng/cm*^{2}) of adsorbed protein in each state. A_{av} is the surface area (*cm*^{2}) available for adsorption, which is given by

$$A_{av} = A_{total}\left(1 - f\sigma_\alpha\rho_\alpha - fb\sigma_\alpha\rho_\alpha\right) \quad (20)$$

where $b = \sigma_\beta / \sigma_\alpha$ and $f = N_A / M$. Since $\theta_i = \sigma_i f \rho_i$ this expression can be written as $A_{av} = A_{total}\left(1 - \theta\right)$, where $\theta = \theta_\alpha + \theta_\beta$. Equations 18 and 19 can be written in terms of fractional surface coverage by multiplying both sides by $\sigma_i f$ to obtain

$$\frac{d\theta_\alpha}{dt} = k_a\sigma_\alpha A_{total} fc\left(1-\theta\right) - k_s A_{total}\theta_\alpha\left(1-\theta\right) - k_d\theta_\alpha \quad (21)$$

$$\frac{d\theta_\beta}{dt} = k_s A_{total} b\theta_\alpha\left(1-\theta\right) \quad (22)$$

When written in this form it is clear that this model utilizes the Langmuir blocking function with $\theta_\infty = 1$. Equations 21 and 22 have the same form as equations 14 and 15 with the rate constants scaled by constant factors.

References

[54] Corning SMF-28e Optical fiber product information. Corning, NY: Corning Incorporated; 2007.

[55] Akimoto T, Sasaki S, Ikebukuro K, Karub I. Refractive-index and thickness sensitivity in surface plasmon resonance spectroscopy. Appl Opt 1999;38:4058–64.

[56] Vörös J. The density and refractive index of adsorbing protein layers. Biophys J 2004;87:553–61.